

Artefacts due to bandpass mis-match

J. Patrick Leahy

University of Manchester

E-mail: jpl@jb.man.ac.uk

Karen Foley

National University of Ireland, Maynooth

E-mail: karen.foley@nuim.ie

Because of their large fractional bandwidth, CMB detectors do not map the sky at a well-defined frequency. If calibrated on the CMB dipole, the resulting maps are accurate for CMB emission, but not for foregrounds which have a different spectrum. Hence:

- Calibrated maps from different detectors at the same nominal frequency will not be consistent;
- Measurements of the foreground spectrum must allow for the bandwidth-induced errors in each detector (which depend on both the bandpass $g(\nu)$ and on the spectral index β);
- Differences between the bandpasses for the two polarizations in a detector lead to non-cancellation of the foreground total intensity in the 'a' - 'b' signal, and hence to a spurious polarization.

We show that, in some ways, the response of the radiometers to continuum emission is remarkably insensitive to the detailed bandpass structure, and can be modelled to high precision with an elementary 'top-hat' bandpass shape. However, it is not possible to accurately match the model parameters of different radiometers, leading to residual errors which can only be removed in tandem with modelling the foreground emission. We illustrate these effects by estimating their amplitude for the *Planck* LFI 30 GHz channel.

CMB and Physics of the Early Universe

20-22 April 2006

Ischia, Italy

1. Formalism

Modern high-gain, high-bandwidth radiometers display substantial structure in their gain-frequency curve (the bandpass, $g(\nu)$), due to internal resonances (Fig. 1, see also [1]). For an input spectrum $T_A(\nu)$, the observed uncalibrated signal is $\int g(\nu) T_A(\nu) d\nu$. To ensure that the calibrated output is equal to the input antenna temperature at the nominal frequency ν_0 , when observing CMB fluctuations (writing $\Delta T_A = \eta_{\Delta T}(\nu) \Delta T$), we require

$$T_{\text{cal}} = \eta_{\Delta T}(\nu_0) \frac{\int g(\nu) T_A(\nu) d\nu}{\int g(\nu) \eta_{\Delta T}(\nu) d\nu} \quad (1.1)$$

For any detector observing emission with $T_A = k\nu^\beta$, there is an effective frequency $\nu_{\text{eff}}(\beta)$ for which the temperature scale is correct, $T_{\text{cal}}(\nu_0 = \nu_{\text{eff}}) = T_A(\nu_{\text{eff}})$. Fig. 2 shows numerical solutions for $\nu_{\text{eff}}(\beta)$ for the example bandpasses of Fig. 1. But we cannot measure β precisely, so even if we set $\nu_0 = \nu_{\text{eff}}(\beta_0)$ for a typical foreground spectral index β_0 , there is a residual gain error $f(\beta)$. Because the assumed foreground spectrum is very smooth, $f(\beta)$ can be accurately represented by a quadratic, as Fig. 3 shows, despite the complex structure of the bandpass.

1.1 Analytic Model

For a sharply cut off bandpass (limits ν_1 and ν_2), with arbitrary slope across the band, assuming a locally power-law spectrum for the CMB,

$$f(\beta) \approx (\beta - \beta_{\text{CMB}}) \left[\varepsilon + \frac{b^2}{24} (\beta - \beta_0) \right] \quad (1.2)$$

where ε is the fractional offset between ν_0 and $\nu_{\text{eff}}(\beta_0)$, and $b = \ln(\nu_2/\nu_1)$ is the fractional bandwidth. Hence a frequency offset gives artefacts linearly proportional to the spectral index difference from the CMB, while the finite bandwidth causes curvature in $f(\beta)$. For a real bandpass we can take b and β_{CMB} as adjustable parameters: for our examples $b \sim 1.2(\Delta\nu/\nu)$ where $\Delta\nu$ is the usual

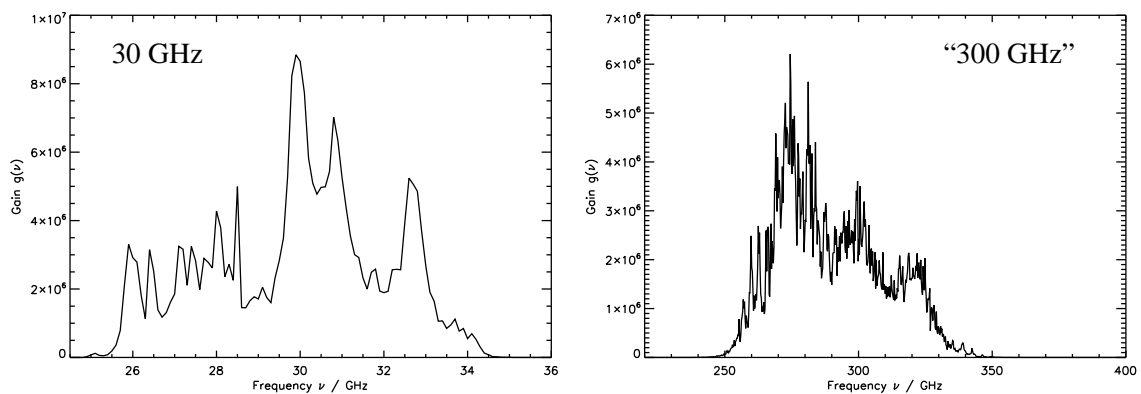


Figure 1: Examples of radiometer bandpasses $g(\nu)$ on a linear scale to emphasise the detailed structure (data courtesy D. Kettle). (a) Left: Prototype *Planck* 30 GHz system. (b) Right, another bandpass artificially scaled to a nominal frequency of 300 GHz. The detailed structure varies from unit to unit, yielding different effective gains for foreground emission in each device.

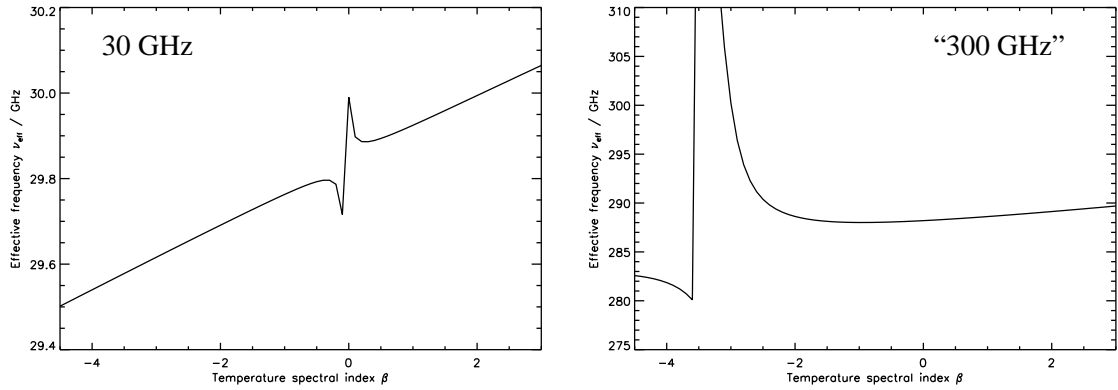


Figure 2: v_{eff} vs. β for our example bandpasses. Anomalous structure occurs when β is close to that of the CMB fluctuations (note the steep T_A spectrum of the CMB at 300 GHz): since the calibration is frequency-independent for the CMB, the effective frequency for similar spectra depends strongly on the detailed shape of the bandpass (and is multi-valued; we select the solution closest to the nominal frequency); however the residual gain error is then insensitive to v_{eff} .

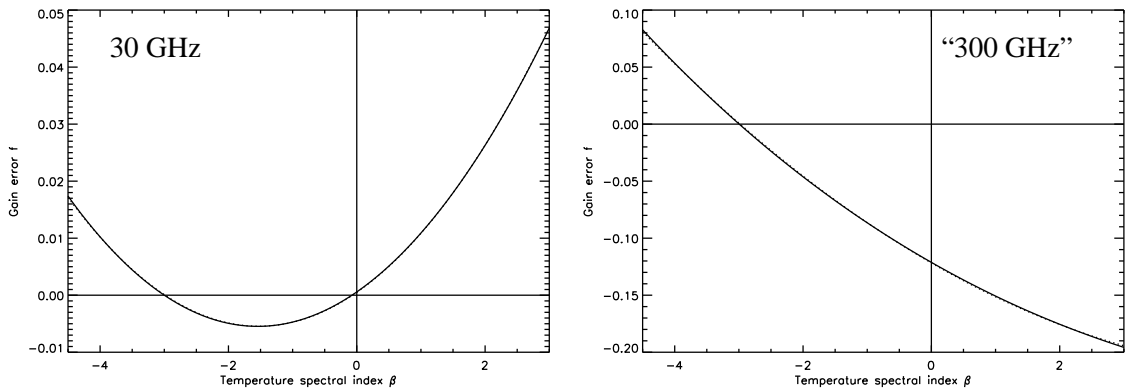


Figure 3: Residual errors $f(\beta)$ for our example bandpasses. (a) Left: For the ‘30 GHz’ bandpass, v_0 is chosen to equal $v_{\text{eff}}(\beta = -3)$, in order to give minimum residual errors for synchrotron emission. (b) Right: For the “300 GHz” bandpass we set v_0 to the target value of 300 GHz, ignoring the fact that $v_{\text{eff}} = 285\text{--}290$ GHz for reasonable β . The offset from v_{eff} gives a large linear gradient in $f(\beta)$. Solid lines are exact calculations from numerical integration across the measured bandpass; close inspection will also reveal dotted lines, which are parabolic fits and almost exactly overlay the accurate curves.

effective bandwidth. The apparent β_{CMB} is close to the actual gradient of the CMB spectrum at 30 GHz, but less so at high frequencies, due to spectral curvature within the band.

2. Multiple Detectors: T vs P

In maps of T made by averaging the results from several detectors, if we assign a nominal frequency equal to the average v_{eff} , we have $\langle \epsilon \rangle = 0$ and so the residual bandpass errors should be proportional to $b^2/24$ and have the parabolic form of Fig. 3a. In contrast, in polarization maps, derived from differences between detector outputs (native Stokes $Q = [T(a) - T(b)]/2$), the b^2 term

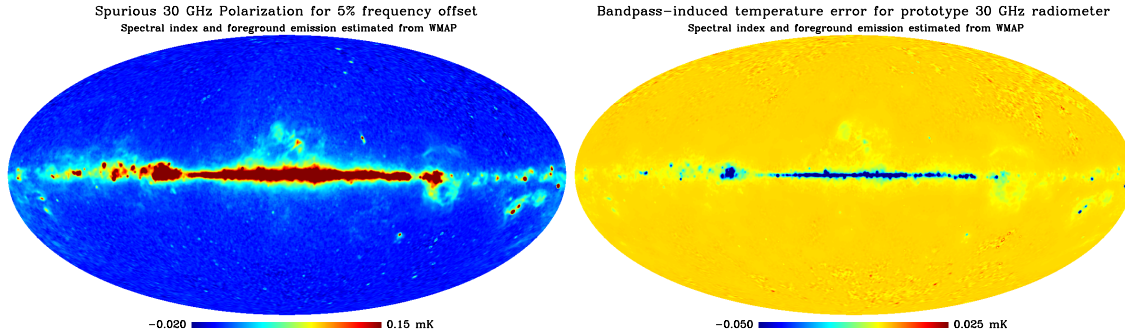


Figure 4: (a) Left: Polarization errors at 30 GHz assuming a 5% offset between v_{eff} for the ‘a’ and ‘b’ polarization radiometers. (b) Right: Temperature error expected at 30 GHz based on *WMAP* data assuming the bandpass in Fig. 1a and v_0 as in Fig. 3a.

will approximately cancel, so the error term will be proportional to $\Delta\epsilon/2$ and be quasi-linear as in Fig. 3b. For the LFI we expect $\Delta\epsilon \sim 3\%$, cf. $b^2/24 \sim 0.2\%$, so the spurious polarization is by far the larger artefact, even before accounting for the much weaker signal in P . For the HFI, since the same filter defines the bandpass for both polarizations, we expect $f(a) - f(b)$ to be almost zero, except for the small frequency dependence of the beam and bolometers, giving very small bandpass errors in P .

2.1 Estimated Error Amplitudes

We estimated the foreground spectral index distribution from the *WMAP* 3-year data, and calculated the bandpass-induced errors in T and P for the LFI at 30 GHz, assuming $b = 0.25$ as for the bandpass in Fig 1a, and $\Delta\epsilon = 5\%$. These errors have rms, outside the *WMAP* Kp2 mask, of $0.7 \mu\text{K}$ in temperature and $6.3 \mu\text{K}$ in native Q .

From the amplitude of the spurious polarization detected by *WMAP* [2, 3], we estimate frequency offsets of $\sim 1\%$ between their two polarization channels. Improved estimates of the *WMAP* polarization could be obtained by using our formalism to find one frequency offset for each differencing assembly, instead of deriving an independent spurious polarization signal at each of 3072 pixels for each assembly. Our approach is required for *Planck*, since each pixel is only observed with two scan angles (quite similar ones for most pixels), so we cannot use the *WMAP* technique of identifying the spurious polarization as a native- Q signal independent of scan angle.

Acknowledgements We thank D. Kettle for providing the bandpass data. K.F. thanks the EU for a Marie Curie Training Fellowship.

References

- [1] Jarosik, N. et al. 2003. *ApJS*, 145, 413
- [2] Jarosik, N. et al. 2006. *ApJ*, submitted, astro-ph/0603452
- [3] Page, L. et al. 2006. *ApJ*, submitted. astro-ph/0603450